

Weak-disorder-induced reduction of the lasing threshold in periodic systems

K. Shadak Alee, Randhir Kumar, and Sushil Mujumdar*

Nano-optics and Mesoscopic Optics Laboratory, Tata Institute of Fundamental Research, 1 Homi Bhabha Road, Mumbai 400 005, India

(Received 16 February 2015; published 13 May 2015)

We report numerical and experimental results on a finite-size, weakly disordered, amplifying multilayer with underlying periodicity. Computed transmission spectra evidence the simultaneous existence of perturbed band-edge modes and random lasing modes in exclusive configurations of disorder. A larger energy is seen to outcouple through the random lasing modes as compared to the band-edge lasing modes. With the gain being uniform across the band gap, this phenomenon originates from the increased quality factor of modes by the addition of disorder. Experiments carried out on a linear array of weakly disordered microresonators exhibit excellent agreement with the numerical observations, demonstrating threshold reduction by the addition of disorder in a periodic system.

DOI: [10.1103/PhysRevA.91.053818](https://doi.org/10.1103/PhysRevA.91.053818)

PACS number(s): 42.55.Zz, 42.25.Dd, 42.25.Hz

Obtaining novel microlaser sources is an attractive proposition in photonics. Recently, a great deal of effort has been focused on periodic systems as templates for microlaser designs. An ordered structure for light constituting periodically arranged low and high dielectric materials, forming a photonic crystal [1,2], realizes passbands and stop bands. Any defects introduced in the periodic structures leads to lasing over the defect states [3–5]. Even in the absence of defects, an amplifying photonic crystal exhibits band-edge lasing when the gain profile suitably supports the band structure [6–9]. On the opposite end of periodicity lies disorder. The complete lack of periodicity realizes disorder, which, rather counterintuitively, can also generate coherent emission. These systems, called random lasers, rely on distributed feedback from elements that are random in either the position or the refractive index [10–14]. A large body of evidence exists on the fascinating physics of random lasers [15–28]. Between the periodic and the disordered regimes lies an intriguing domain wherein randomness exists, albeit with a certain degree of periodicity. The studies of such periodic-on-average random systems have produced interesting features of light transport [16,29–35].

In random systems with underlying periodicity, states arise in the band gap, whose Q factor is high owing to the remnant Bragg reflection from the erstwhile periodic elements. Experimental research has revealed disorder-induced lasing in inverse opals [29,36–39]. However, the threshold behavior in such studies is often connected to the position of the gain maximum with respect to the band gap. Indeed, the gain profile can enhance the intensity of modes closest to the gain maximum, an effect that is less connected to the quality factor of the modes. It is desirable to disconnect the influence of the gain profile in order to understand the contribution of the disorder-induced modes, since many intriguing theoretical observations exist related to the modal behavior. For instance, one such numerical investigation revealed that the Q factor is maximized at an optimal degree of disorder [40]. In this case, the modes are of a higher Q than even the band-edge modes. This immediately implies a lowered threshold for the random laser modes in comparison

to band-edge laser modes. However, this interesting inference has not been experimentally verified so far, because of several critical requirements. First, the gain profile needs to be flat across the gap. Second, the system should generate band-edge modes and random lasing modes in a clear distinguishable manner. Finally, since the field of disordered systems requires statistically complete measurements, the system should offer many configurations to draw reliable conclusions. In this paper we experimentally achieve all the aforementioned conditions of disorder with sufficient precision and obtain conclusive data. First, we numerically examine the threshold fluctuations in a finite-size, one-dimensional periodic-on-average system with weak disorder. We observe that certain configurations exhibit random lasing (RL) modes with low thresholds, while other configurations realize perturbed band-edge (PBE) states with higher thresholds. This observation is commensurate with the theoretical studies presented by Apalkov and Raikh [41] for finite-size random lasers. There it was shown that, at a given disorder strength, threshold fluctuations originate from the probabilistic occurrence of highest- Q modes among the various random resonators. In our system with weak disorder, certain configurations are periodic enough such that the band-edge modes have the highest Q . On the other hand, other configurations sustain random lasing modes that are of the highest quality. Finite-difference time domain simulations with gain are used to study the effect of the threshold behavior on the output intensity. We experimentally verify this behavior in a linear array of microresonators, where the intensity of random lasing modes and the fluctuations thereof are indeed seen to be higher than the perturbed band-edge modes, in excellent agreement with the computations. This work provides a direct and systematic experimental report where lowering of threshold in random lasing as compared to band-edge lasing is demonstrated.

We first analyze the transmission characteristics of a one-dimensional system, or a multilayer. These numerical investigations involve one-dimensional transfer matrix calculations with gain, where the gain is modeled by a negative imaginary refractive index, independent of wavelength. The system comprises 40 layers, with alternating active and passive layers, with an average gain layer thickness A of 20 μm and passive layer thickness B of 8 μm . The refractive indices of the two layers are 1.41 and 1.0, respectively, as motivated

*mujumdar@tifr.res.in; <http://www.tifr.res.in/~mujumdar>

by our experimental system, discussed later. Here δA and δB represent the widths of the Gaussian distributions about A and B , which quantify the disorder. Figure 1(a) depicts the calculated lasing threshold as a function of randomness only in B . The markers represent the average of the first-lasing threshold of 100 configurations at the same strength of randomness and the error bars indicate the distribution in the threshold values. Clearly, the threshold of lasing decreases to a minimum when $\delta B \sim 75$ nm. Essentially, this is the gain counterpart of the previously known result of an increase in modal quality factors at an optimal disorder [40]. Next we investigate various configurations at a given δB . Figure 1(b) shows band-edge lasing from the periodic system ($\delta A = \delta B = 0$), while Fig. 1(c) shows two spectra at $\delta B = 50$ nm. The red spectrum reveals the memory of band edges as clearly shown in the double-mode spectrum, while the blue spectrum shows a single peak in the middle of the band gap, where randomness realizes gap-state lasing. The consequence of this dual behavior is evident in the wavelength distribution of the lasing modes. Figure 1(d) shows the distribution at $\delta B = 50$ nm, wherein a double-peak bunch can be seen at the position of each gap. The distribution is maximized in the vicinity of the band edges of the underlying periodic system ($\delta B = 0$ nm). These bins are occupied by the perturbed band-edge modes. The band structure is shown in purple for reference. Figure 1(e) depicts the situation for stronger disorder ($\delta B = 1 \mu\text{m}$). In this case, the system shows single-peak bunches indicating that the memory of the band edges is eliminated. The modes occupy a larger extent on the wavelength axis. Furthermore, the range of wavelengths is also shifted significantly, because the randomness realizes modes at the minima of the Fabry-Pérot profile (purple curve) of the active layer, a phenomenon that we have already reported earlier [17]. Finally, Fig. 1(f) shows the threshold behavior of the weakly and strongly disordered systems. The vertical green lines demarcate the band gaps in the periodic structure. The four green stars indicate the threshold of the band-edge modes. The blue triangles show the average first-lasing mode thresholds at the respective wavelengths in the strongly random system, where the thresholds are higher than the band-edge threshold at any wavelength. The red circles indicate the thresholds for the weakly random system. Clearly, all the thresholds within the stop band are lower than that of the band-edge modes, while those in the passband are higher. Thus, the gap-state random lasing modes have a lower threshold than the band-edge modes, when the system is weakly disordered.

Experimentally, the intensity, and not the threshold, is a more accessible parameter and hence it is instructive to investigate the behavior of the output intensity in each configuration. Numerical instabilities in transfer matrix computations render them inadequate for quantitative intensity studies above the threshold [15]. Therefore, we resort to finite-difference time domain (FDTD) computations to examine the intensity behavior in such weakly random systems. Figure 2(a) illustrates the schematic of the one-dimensional multilayer studied by FDTD computations (Lumerical Inc). In order to avoid the huge computational cost of FDTD computations, we studied a physically smaller system of total size $23.2 \mu\text{m}$ comprising 16 layers, with the active layer thickness A of 800 nm, passive layer B of 650 nm, and refractive indices 3 and 1, respectively.

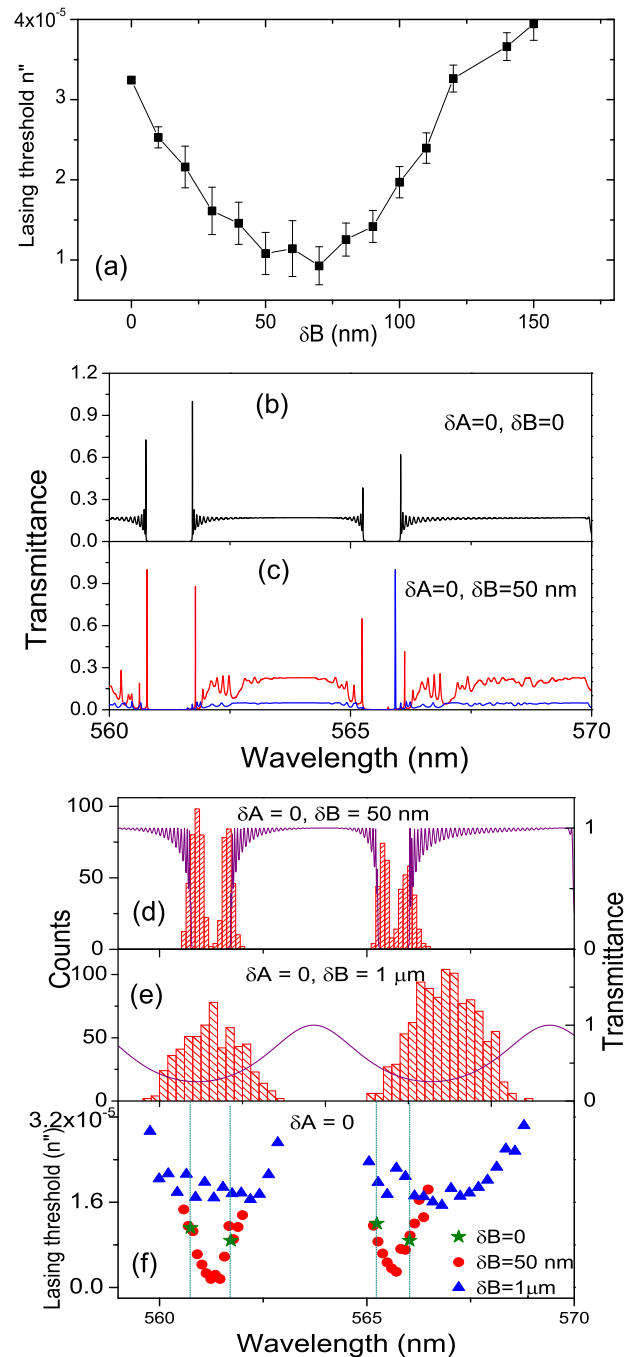


FIG. 1. (Color online) (a) Calculated averaged lasing threshold of the first-lasing mode versus δB ($\delta A = 0$). (b) Band-edge lasing from a periodic multilayer ($\delta A = \delta B = 0$). (c) Spectra from two configurations in a system with $\delta B = 50$ nm, exhibiting perturbed band-edge lasing (red curve) and gap-state random lasing (blue curve). (d) Distribution of lasing wavelengths for the case of $\delta A = 0$ and $\delta B = 50$ nm. The purple line (right Y axis) shows the transmission spectrum of the periodic structure. (e) Corresponding distribution for the case of strong randomness ($\delta A = 0$ and $\delta B = 1 \mu\text{m}$). The purple line (right Y axis) shows the Fabry-Pérot profile of a single layer of thickness A . (f) Wavelength dependence of lasing thresholds. The green stars show the band-edge lasing thresholds for the four modes in (b). Vertical green lines demarcate the stop bands. Red circles and blue triangles represent the thresholds for the weakly and strongly disordered systems, respectively.

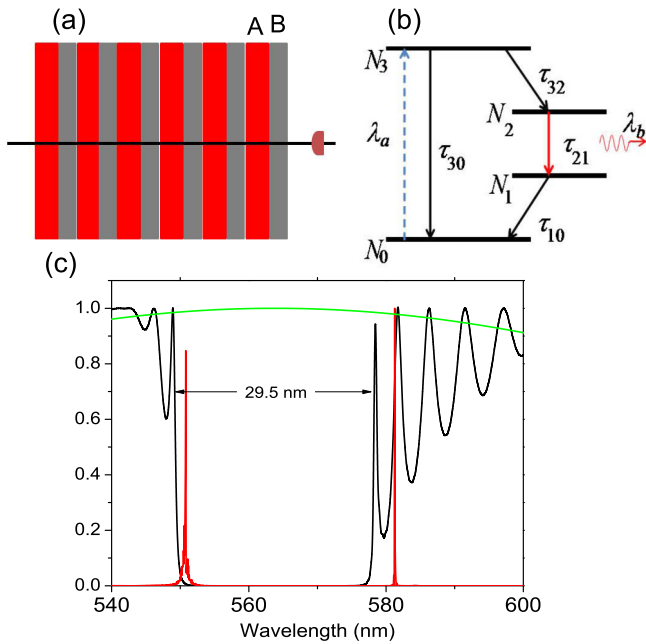


FIG. 2. (Color online) (a) Schematic of the FDTD simulated multilayer, with orange showing the gain layer and the gray the passive layer. (b) Four-level gain scheme implemented for gain in the simulation. (c) The black line shows the passive transmission spectrum of the multilayer and the red line shows the band-edge lasing from the same. The green line shows the gain profile, whose width (~ 168 nm) is much larger than the band gap (29.5 nm).

Absorbing boundary conditions using a perfectly matched layer were implemented to simulate the finite-size nature of the system. Saturable gain was incorporated in dielectric layers using a four-level two-electron model [42], whose scheme is shown in Fig. 2(b). In this model the electrons in the ground state N_0 were pumped to an excited state N_3 using a continuous external pump of $\lambda = 350$ nm. After a short lifetime τ_{32} , the electrons were transferred to the upper laser level N_2 nonradiatively. The lasing occurs between N_2 and the lower lasing level N_1 , after which the electrons drop to the ground state N_0 through nonradiative decay. The lifetimes τ_{32} and τ_{10} were maintained 10 fs, while τ_{30} and τ_{21} were 300 ps. The linewidths of pump and lasing transitions γ_a and γ_b were chosen to be 10^{13} and 10^{15} s^{-1} , respectively. The maximum of the gain profile [Fig. 2(c), green curve] was centered at the middle of the stop band at 565 nm and with a width of ~ 168 nm it was much wider than the band gap (width of 29.5 nm), thus realizing an almost flat gain profile. The ground level electron density was chosen to be 1.5×10^{25} m^{-3} . The lasing intensity for every configuration was taken after reaching its steady-state value, measured at a point detector after the structure. The threshold for each mode was determined by monitoring the input-output intensity curve. An appropriate disorder strength, which would manifest perturbed band-edge modes, was incorporated in the passive layer thickness. Figure 2(c) depicts the passive spectrum (black curve) from this sample. For the chosen parameters, a single wide stop band resulted in the wavelength range examined. The red curve shows the band edge lasing spectrum from this periodic sample. The band-edge modes are redshifted from

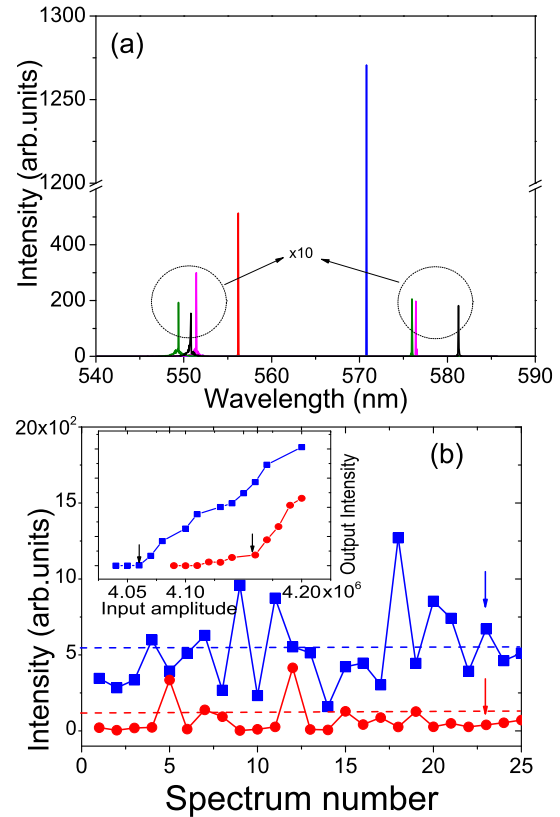


FIG. 3. (Color online) (a) Five spectra calculated using the FDTD with gain are shown. Black lines show the band-edge spectrum from the periodic system. Magenta and green lines show perturbed band-edge modes from a weakly random system. Red and blue peaks show random lasing modes from two configurations of the weakly random system. (b) Intensity behavior over several (25) configurations is shown. Blue markers indicate the intensity of the random lasing modes, while red markers show the total intensity coupled into the two PBE modes. The inset shows the input-output curves for two configurations marked by arrows, showing the respective thresholds. Red curve indicates the first-lasing PBE mode for the configuration.

the passive band edges, as expected from the Kramers-Kronig relation [15,43].

Next we computed the intensity behavior from 100 random configurations of the sample. Figure 3(a) depicts four spectra from this system, apart from the band-edge lasing spectrum (black line). The green and magenta spectra are two PBE lasing spectra from two configurations. The red and blue peaks correspond to two RL spectra. The random lasing modes exhibit a large emission intensity compared to the rest, which are already enhanced by a factor of 10. Figure 3(b) shows the intensity behavior of several spectra, with the red markers showing the total PBE mode intensity (sum of the two PBE modes) and the blue spectra showing the RL intensity. The inset shows the input-output curve illustrating the threshold behavior of two modes in the series, identified by arrows. The lower threshold of the random lasing spectrum is immediately evident, which manifests a higher emission intensity.

Motivated by these calculations, experiments were implemented on a periodic-on-average random system that we have

demonstrated earlier [16]. A linear array of microspheres was obtained using a vibrating orifice aerosol generator (VOAG) that creates microdroplets of a liquid medium, using the fracture of an unstable liquid jet [44]. When this unstable jet is subjected to an appropriate periodic perturbation, it can be induced to break up into equal-size droplets. In our setup, the jet is realized by a microcapillary, while the perturbation is created by a piezoelement inside the capillary to which a periodic voltage is applied. Since the current experiments required a higher degree of periodicity than what we had achieved earlier, two simple but effective modifications were implemented. First, the microdroplets were created from a rhodamine 6G solution in ethylene glycol instead of methanol, and second, they were produced in an evacuated chamber. The viscous nature of the solvent (ethylene glycol) and the vacuum helped in reducing the fluctuations in size and spacing. Around 20 microdroplets were illuminated under the pump laser spot. Along the axis of this linear array, the refractive index profile resembles a multilayer. The transverse (perpendicular to the array) emission and the longitudinal emission were separately analyzed by a spectrometer (Czerny-Turner, with a focal length of 50 cm). The longitudinally traveling light experiences the multilayer arrangement, whose widths and separations can be tweaked by modifying the pressure and piezofrequency of the VOAG. Further details of the sample characterization and experimental techniques are described in Ref. [45].

Figure 4 represents the experimental results from the system. Figure 4(a) depicts the image of the microdroplet array and the axial refractive index profile underneath. A very high degree of periodicity is visible in the image. This was also ascertained from analysis of whispering gallery modes of the microspheres, which showed a monodispersity δA within 80 nm, for a diameter A of $17.3 \mu\text{m}$. From the images of the array, the average spacing B was estimated to be approximately $7.8 \mu\text{m}$. The fluctuations δB were too small to be quantified accurately from the images. In the fluid-dynamic generation process of the VOAG, the fluctuations in the periodicity in the array are concomitant with those in the diameter of the microdroplets. Thus, the extreme monodispersity in the diameters implies a large underlying periodicity. The fact that we achieved the appropriate degree of randomness was evident from the spectra and distributions. Indeed, certain configurations exhibited doublet spectra originating from perturbed band-edge modes. At the same time, other configurations were random enough to sustain single random lasing peaks. Importantly, the gain profile of the dye is much broader ($\sim 40 \text{ nm}$) than the band gap ($\sim 1 \text{ nm}$), ensuring that the observations are not influenced by the gain maximum. Figure 4(b) shows two PBE spectra (black and red lines) and two RL spectra in the middle of the gap (green and blue lines). In the plot the red line spectrum is vertically offset to avoid clutter. These spectra were obtained under a pump energy of $0.3 \mu\text{J}$. The intensity of the RL modes is clearly higher than the PBE modes. The inset shows spectra (vertically offset) when the randomness was larger, $\delta B = 1 \mu\text{m}$. Figure 4(c) depicts the histogram of the lasing wavelengths, clearly illustrating two peaks in the bunch, as was anticipated from the transfer matrix computations [Fig. 1(c)]. The peaks of this distribution coincide with the PBE modes. For comparison, the inset shows a single-peak bunch of the random sample.

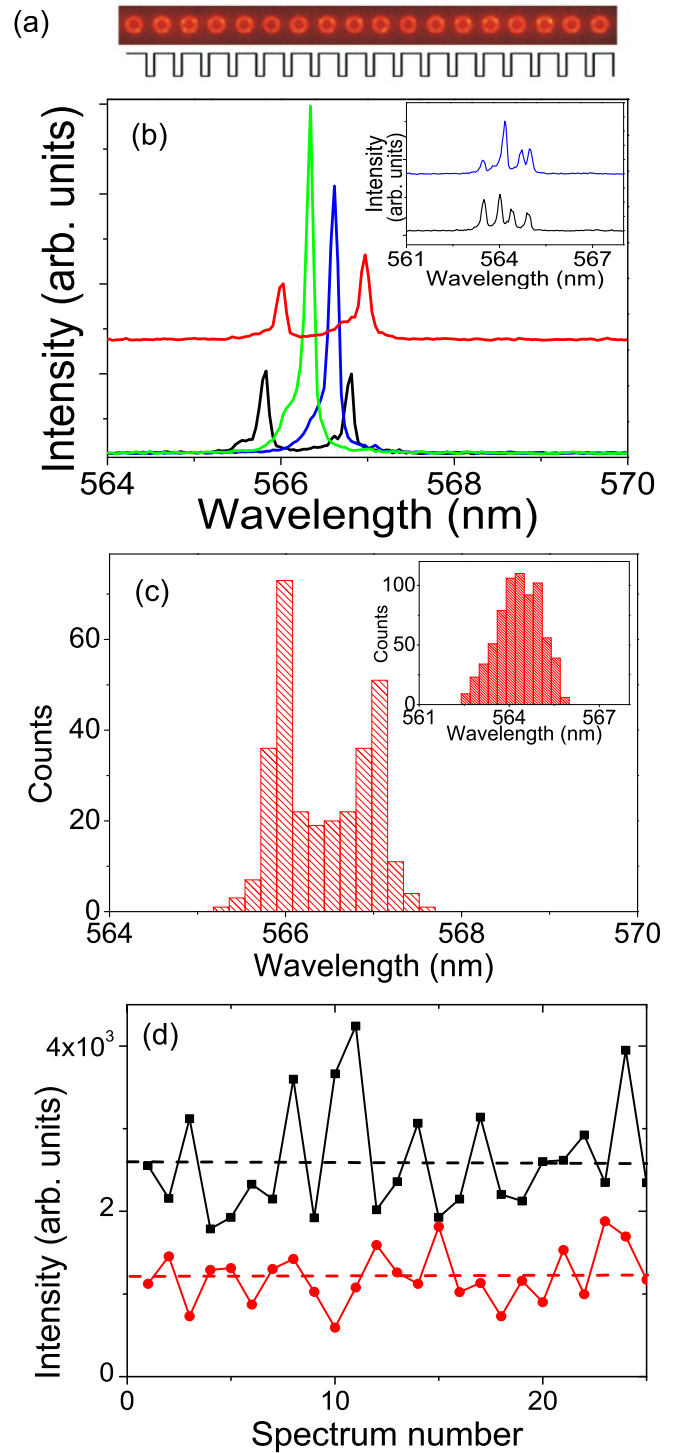


FIG. 4. (Color online) (a) Image of the microdroplet array along with the axial refractive index underneath. (b) Two representative spectra of perturbed band-edge lasing (black and red lines) and two random lasing spectra (blue and green lines) obtained from the system. Only the red spectrum is offset vertically for clarity. The inset shows two spectra (offset vertically for clarity) at larger disorder ($\delta B = 1 \mu\text{m}$). (c) Histogram of the lasing wavelengths, showing a two-peaked distribution. The inset shows a single-peak histogram when $\delta B = 1 \mu\text{m}$. (d) Peak intensities of random (black squares) and perturbed band-edge (red circles) lasing modes, in clear agreement with computational results.

Next we quantified the intensity channeled into the PBE modes and single peaks of RL modes over several pulses. In Fig. 4(d) the intensity of the two PBE modes is summed and plotted with the spectrum number as red dots. The intensity of the single-peak random lasing modes is displayed as black dots. Clearly, the average intensity of the random lasing modes (black dashed line) is larger by a factor of 2.2 compared to the average intensity coupled into perturbed band-edge lasing (red dashed line). These observations are in excellent agreement with the FDTD computations of Fig. 3(b), where the lower thresholds of the random lasing modes realizes such a behavior. The low thresholds are a direct consequence of the high-quality factors of the gap states as compared to the band-edge states. This may be qualitatively understood from the basic functioning of a multilayer. Periodicity in a multilayer realizes two band-edge modes (at one stop band) that have the same, or at least very comparable, quality factors. The partial reflections from the various interfaces in the multilayer act in tandem so

as to sustain these two modes. In contrast, the random system manifests only one mode in the gap. In this case, the same number of interfaces needs to sustain only one mode, thus raising the efficacy of the interference of all partial reflections, leading to an increased quality factor of the mode. In the presence of amplification, this leads to a reduced threshold.

In summary, we have experimentally demonstrated the threshold behavior of a random laser at weak randomness in the presence of underlying periodicity. The finite size of the sample realizes perturbed band-edge lasing modes and random lasing modes in different configurations. The intensity coupled into the RL modes is larger, owing to the lower threshold in the middle of the energy gap. These studies should enable more research towards novel lasing sources, particularly those based on the synergy of periodicity and disorder.

S.M. acknowledges support from the DAE, Government of India, and the DST for the Ramanujan Fellowship.

-
- [1] E. Yablonovitch, *Phys. Rev. Lett.* **58**, 2059 (1987).
 [2] S. John, *Phys. Rev. Lett.* **58**, 2486 (1987).
 [3] O. Painter, R. K. Lee, A. Scherer, A. Yariv, J. D. O'Brien, P. D. Dapkus, and I. Kim, *Science* **284**, 1819 (1999).
 [4] R. Ozaki, Y. Matsuhisa, M. Ozaki, and K. Yoshino, *Appl. Phys. Lett.* **84**, 1844 (2004).
 [5] J. Yoon, W. Lee, J. M. Caruge, M. Bawendi, E. L. Thomas, S. Kooi, and P. N. Prasad, *Appl. Phys. Lett.* **88**, 091102 (2006).
 [6] M. Meier, A. Mekis, A. Dodabalapur, A. Timko, R. E. Slusher, J. D. Joannopoulos, and O. Nalamasu, *Appl. Phys. Lett.* **74**, 7 (1999).
 [7] A. Mekis, M. Meier, A. Dodabalapur, R. E. Slusher, and J. D. Joannopoulos, *Appl. Phys. A* **69**, 111 (1999).
 [8] V. I. Kopp, B. Fan, H. K. M. Vithana, and A. Z. Genack, *Opt. Lett.* **23**, 1707 (1998).
 [9] R. V. Nair, A. K. Tiwari, S. Mujumdar, and B. N. Jagatap, *Phys. Rev. A* **85**, 023844 (2012).
 [10] D. S. Wiersma, *Nat. Phys.* **4**, 359 (2008).
 [11] H. Cao, *J. Phys. A: Math. Gen.* **38**, 10497 (2005).
 [12] V. S. Letokhov, *Sov. Phys. JETP* **26**, 835 (1968).
 [13] N. M. Lawandy, R. M. Balachandran, A. S. L. Gomes, and E. Sauvain, *Nature (London)* **368**, 436 (1994).
 [14] M. Noginov, *Solid State Random Lasers*, Springer Series in Optical Sciences Vol. 105 (Springer, New York, 2005).
 [15] J. Andreasen, A. A. Asatryan, L. C. Botten, M. A. Byrne, H. Cao, L. Ge, L. Labontè, P. Sebbah, A. D. Stone, H. E. Türeci, and C. Vanneste, *Adv. Opt. Photon.* **3**, 88 (2011).
 [16] A. K. Tiwari and S. Mujumdar, *Phys. Rev. Lett.* **111**, 233903 (2013).
 [17] A. K. Tiwari, K. S. Alee, R. Uppu, and S. Mujumdar, *Appl. Phys. Lett.* **104**, 131112 (2014).
 [18] N. Bachelard, S. Gigan, X. Noblin, and P. Sebbah, *Nat. Phys.* **10**, 426 (2014).
 [19] J. Fallert, R. J. B. Dietz, J. Sartor, D. Schneider, C. Klingshirn, and H. Kalt, *Nat. Photon.* **3**, 279 (2009).
 [20] S. Gottardo, R. Sapienza, P. D. García, A. Blanco, D. S. Wiersma, and C. López, *Nat. Photon.* **2**, 429 (2008).
 [21] M. Leonetti, C. Conti, and C. Lopez, *Nat. Photon.* **5**, 615 (2011).
 [22] A. Tulek, R. C. Polson, and Z. V. Vardeny, *Nat. Phys.* **6**, 303 (2010).
 [23] H. E. Türeci, L. Ge, S. Rotter, and A. D. Stone, *Science* **320**, 643 (2008).
 [24] S. K. Turitsyn, S. A. Babin, A. E. El-Taher, P. Harper, D. V. Churkin, S. I. Kablukov, J. D. Ania-Castañón, V. Karalekas, and E. V. Podivilov, *Nat. Photon.* **4**, 231 (2010).
 [25] R. Uppu and S. Mujumdar, *Opt. Lett.* **35**, 2831 (2010).
 [26] R. Uppu and S. Mujumdar, *Phys. Rev. A* **87**, 013822 (2013).
 [27] R. Uppu and S. Mujumdar, *Phys. Rev. A* **90**, 025801 (2014).
 [28] R. Uppu and S. Mujumdar, *Phys. Rev. Lett.* **114**, 183903 (2015).
 [29] P. D. Garcia and C. Lopez, *J. Mater. Chem. C* **1**, 7357 (2013).
 [30] J. F. Galisteo-Lopez, M. Ibisate, R. Sapienza, L. S. Froufe-Pérez, Á. Blanco, and C. López, *Adv. Mater.* **23**, 30 (2011).
 [31] C. Conti and A. Fratlocchi, *Nat. Phys.* **4**, 794 (2008).
 [32] L. I. Deych, D. Zaslavsky, and A. A. Lisyansky, *Phys. Rev. Lett.* **81**, 5390 (1998).
 [33] A. R. McGurn, K. T. Christensen, F. M. Mueller, and A. A. Maradudin, *Phys. Rev. B* **47**, 13120 (1993).
 [34] G. M. Conley, M. Burrese, F. Pratesi, K. Vynck, and D. S. Wiersma, *Phys. Rev. Lett.* **112**, 143901 (2014).
 [35] L. Dal Negro and S. V. Boriskina, *Laser Photon. Rev.* **6**, 178 (2012).
 [36] M. Scharrer, H. Noh, X. Wu, M. A. Anderson, A. Yamilov, H. Cao, and R. P. H. Chang, *J. Opt.* **12**, 024007 (2010).
 [37] M. N. Shkunov, M. C. DeLong, M. E. Raikh, Z. V. Vardeny, A. A. Zakhidov, and R. H. Baughman, *Synth. Met.* **116**, 485 (2001).
 [38] M. N. Shkunov, Z. V. Vardeny, M. C. DeLong, R. C. Polson, A. A. Zakhidov, and R. H. Baughman, *Adv. Funct. Mater.* **12**, 21 (2002).
 [39] L. K. Teh, C. C. Wong, H. Y. Yang, S. P. Lau, and S. F. Yu, *Appl. Phys. Lett.* **91**, 161116 (2007).

- [40] A. Yamilov and H. Cao, *Phys. Rev. A* **69**, 031803(R) (2004).
- [41] V. M. Apalkov and M. E. Raikh, *Phys. Rev. B* **71**, 054203 (2005); **72**, 189903(E) (2005).
- [42] A. Taflove and S. Hagness, *Computational Electrodynamics: The Finite-Difference Time-Domain Method*, 3rd ed. (Artech House, Norwood, 2005).
- [43] The modified real part of the refractive index $n'_r = \sqrt{n_r^2 + n_i^2}$, where n_r and n_i represent the original real part and the gain-induced imaginary part, respectively.
- [44] H. B. Lin, J. D. Eversole, and A. J. Campillo, *Rev. Sci. Instrum.* **61**, 1018 (1990).
- [45] A. K. Tiwari, B. Chandra, R. Uppu, and S. Mujumdar, *Opt. Express* **20**, 6598 (2012).